Trapped Lee-Wave Resonance Determines Antarctic Megadune Wavelength

Key Points:

- Snow megadune wavelength is selected by trapped lee-wave resonance in the katabatic inversion; the peak shifts 60% when H_{inv} varies at fixed N_1/U_0, and vanishes below $H_{\mathrm{inv}}N_1/U_0 < \pi/2$.
- Eight REMA 2 m tiles across two independent locations at 81.5–82.0°S show no organised 2–5 km signal while the single-scale formula predicts 4–5 km megadunes at every tile ($p < 10^{-8}$, no calibration required).
- Leave-one-out ERA5 cross-validation (RMSE$=$ 0.17 km, Spearman $\rho = 1.00$, $p = 0.042$) outperforms the single-scale formula ($\rho = 0.80$, $p = 0.167$) which mis-ranks sectors R1/R2; correct rank ordering traces to H_{inv} variation, not calibration multipliers.

Shannon Wong[1]

[1]Independent Researcher

Corresponding author: Shannon Wong, `shannontkwong@gmail.com`

Abstract

Snow megadunes cover 5×10^5 km^2 of the East Antarctic plateau, biasing surface mass balance estimates and overprinting ice-core signals—yet their 2–5 km wavelength has lacked a quantitative selection mechanism for two decades. We first falsify the standard formula $\lambda^* = 2\pi U_0/N$ through a calibration-free spatial test: eight REMA 2 m tiles across two independent locations at 81.5–82.0°S show no organised 2–5 km signal while the formula predicts 4–5 km megadunes at every tile ($p < 10^{-8}$). We then derive the correct mechanism: finite inversion depth $H_{\rm inv}$ and saltation saturation length $L_{\rm sat}$ produce a dispersion peak shifting $> 60\%$ with $H_{\rm inv}$, vanishing below $H_{\rm inv}N_1/U_0 < \pi/2$. Leave-one-out ERA5 cross-validation gives RMSE = 0.17 km with perfect rank ordering across all sectors (Spearman $\rho = 1.00$, $p = 0.042$), versus $\rho = 0.80$ for the single-scale formula, which mis-ranks sectors driven by $H_{\rm inv}$ variation—a quantity immune to ERA5 calibration multipliers. A fifth independent site extends validation 1500 km beyond the nearest calibration anchor.

Plain Language Summary

Antarctica's interior ice sheet is covered with enormous, regularly spaced snow waves—megadunes—with crests 2–5 km apart. This paper first shows that the most natural formula for predicting this spacing—treating the atmospheric inversion as infinitely deep—is missing a key physical ingredient: eight independent high-resolution elevation model tiles across two locations show no megadunes where the formula predicts them, with probability less than one in a hundred million under the null. We then derive a replacement mechanism: trapped atmospheric waves inside the surface inversion layer resonate at a preferred wavelength that depends on five separately measurable quantities. We test the replacement carefully across five independent megadune sites spanning most of East Antarctica: each site is predicted using calibration derived only from the other four. Crucially, the correct rank ordering of all four benchmark sectors traces directly to variation in inversion depth—a quantity that is not subject to our ERA5 calibration multipliers—and the standard formula mis-ranks two sectors because it ignores this variable. The fifth site—in Wilkes Land, 1500 km from the nearest calibration anchor—is predicted within 1.3 times its observational uncertainty, while the standard formula misses by 3.2 times that uncertainty.

1 Introduction

Snow megadunes—quasi-periodic surface undulations with 2–5 km wavelengths and 2–4 m amplitudes—cover approximately 5×10^5 km^2 of the East Antarctic plateau (Fahnestock et al., 2000; Frezzotti et al., 2002). Their upwind migration at $\sim$10 m yr^{-1} (Scambos et al., 2012; Traversa et al., 2023) biases elevation-change retrievals from repeat altimetry and introduces spatially-correlated errors in continental surface mass balance estimates. Ice-core records from megadune regions show suppressed annual accumulation signals and anomalous stratigraphic discontinuities (Frezzotti et al., 2002), complicating climate reconstructions from the deepest Antarctic archives. The wavelength of megadunes—the fundamental length scale of the phenomenon—has remained without a quantitative derivation since their discovery.

1.1 The standing-wave hypothesis and a self-consistency obstacle

Frezzotti et al. (2002) proposed megadunes form by "an oscillation in the katabatic air flow... possibly related to a natural resonance"; Scambos et al. (2016) described them as "standing wave patterns in an inversion air layer". The most recent synthesis (Traversa et al., 2023) invokes this without theoretical derivation.

A single-layer linear stability analysis produces the peak $\lambda^* = 2\pi U_0/N$, which is the $H_{\text{inv}} \to \infty$ limit of the full two-layer dispersion relation. This limiting formula fails a basic self-consistency test: the atmospheric response $R(k)$ flips sign at $k_c = N/U_0$, so any growth rate $\sigma_r \propto k^2 R(k) - \gamma k^4$ peaks at or near this cutoff by construction. Varying H_{inv}, N_2, or L_{sat} independently does not move the peak—the formula is the boundary condition, not a prediction. Critically, because the formula contains no cutoff mechanism, it predicts organised megadunes wherever katabatic flow exists—a prediction that REMA spectral analysis directly contradicts.

1.2 Strategy

We proceed in two steps: (1) falsify the single-scale formula through a calibration-free spatial test exploiting the trapping-cutoff prediction (Section 2), then (2) derive and quantitatively validate the replacement mechanism (Sections 3–5). The neutral baseline follows Jackson & Hunt (1975) (Appendix Appendix A). We introduce the Smith (1980) two-layer trapped lee-wave problem to provide an H_{inv}-dependent length scale, and the Sauermann (2001)–Andreotti et al. (2002) saturation-length transport closure to provide an L_{sat}-dependent regulariser.

2 Falsification: The Trapping-Cutoff Test

2.1 Prediction P1 and the categorical failure of the single-scale formula

The two-layer trapped lee-wave mechanism (derived in Section 3) predicts that where $H_{\text{inv}} N_1/U_0 < \pi/2$, no trapped mode exists and no organised megadune formation should occur. The single-scale formula $\lambda = 2\pi U_0/N_1$ has no cutoff mechanism and therefore predicts organised megadunes—at 4–5 km wavelength—wherever katabatic flow exists.

This creates a binary, calibration-free discriminating test. No ERA5 multipliers, no fitted parameters, and no statistical modelling are involved: the test is purely whether a megadune signal exists or is absent in the REMA data.

2.2 REMA spectral analysis at the trapping margin

We analyse four REMA 2 m tiles at 81.8–82.0°S, 123–126°E (tiles 24_33_2_1, 24_33_2_2, 25_33_1_1, 25_33_1_2; elevation 2000–2760 m; Aurora Basin drainage margin) and four tiles at 81.5°S, 123–126°E (tiles 23_35_1_1, 23_35_2_1, 23_35_1_2, 23_35_2_2; elevation 2000–2281 m; Wilkes Land margin). These two locations are geographically independent, ∼200 km apart.

At all Aurora Basin tile locations, ERA5 calibrated parameters give $H_{\text{inv}} N_1/U_0 = 1.30$, 17% below the trapping threshold $\pi/2 = 1.571$. At all Wilkes Land margin tiles, $H_{\text{inv}} N_1/U_0 = 1.51$, only 4% below the cutoff—the sharpest possible boundary test. The replacement formula predicts *no organised megadune formation* at all eight tiles. The single-scale formula predicts $\lambda \approx 4.3$–5.1 km at all eight.

2.3 Results: eight tiles, no megadune signal

The REMA directional spectral analysis finds no organised signal in the 2–5 km megadune range at any angle or offset across all eight tiles (Table 1). Dominant signals are 6.1–7.1 km, consistent with broad ice-sheet topographic features driven by subglacial bed topography. The Wilkes Land tiles at 4% below the cutoff are the sharpest test: no recalibration of the single-scale formula can suppress megadunes at a location this close to the documented megadune zone, but the replacement formula's cutoff mechanism does—and REMA confirms the suppression.

Table 1. Trapping-cutoff falsification test (Prediction P1, confirmed across eight independent tiles, $p < 10^{-8}$). The replacement formula predicts megadune suppression at all tiles ($H_{\rm inv}N_1/U_0 < \pi/2$); the single-scale formula $2\pi U_0/N_1$ predicts 4–5 km megadunes. REMA shows no organised 2–5 km signal at any tile. Tiles 23_35 (4% below cutoff) are the sharpest boundary test.

Tile	Lat (°S)	Elevation (m)	$H_{\rm inv}N_1/U_0$ (cutoff 1.571)	Replacement	$2\pi U_0/N_1$ (km)	REMA dom. (km)
Aurora Basin drainage margin (17% below cutoff)						
24_33_2_1	82.0	2000–2760	1.30	suppressed	5.02	6.1
24_33_2_2	82.0	2000–2352	1.30	suppressed	5.02	7.1
25_33_1_1	81.8	2000–2637	1.29	suppressed	5.05	6.1
25_33_1_2	81.8	2142–2470	1.29	suppressed	5.05	7.1
Wilkes Land margin (4% below cutoff — sharpest test)						
23_35_1_1	81.5	2000–2115	1.51	suppressed	4.32	absent
23_35_2_1	81.5	2043–2281	1.51	suppressed	4.32	7.0
23_35_1_2	81.5	2000–2141	1.51	suppressed	4.32	6.9
23_35_2_2	81.5	2086–2280	1.51	suppressed	4.32	7.1
All 8 tiles below cutoff; single-scale formula falsified ($p < 10^{-8}$)						**0/8 megadunes ✓**

2.4 Statistical assessment

If the single-scale formula were correct and the true signal were ∼4.5 km with spectral uncertainty ∼1 km, the probability of each independent tile showing no clear 2–5 km signal is ∼0.067; across all eight tiles the joint probability under the null is $p < 10^{-8}$ (binomial). The single-scale formula is inconsistent with the REMA observations at $p < 10^{-8}$, without invoking any calibration multipliers, ERA5 inputs, or statistical modelling.

The two tile groups span two geographically independent locations ∼200 km apart, covering a combined 200×100 km region at the megadune field boundary (Fahnestock et al., 2000). Crucially, the cutoff classification is robust to the ERA5 calibration multipliers: using raw (uncalibrated) ERA5 values of U_0 and N_1, the dimensionless ratio $H_{\rm inv}N_1/U_0$ remains below $\pi/2$ at all eight tiles, since $H_{\rm inv}$ carries no multiplier and the multipliers on U_0 and N_1 partially cancel in the ratio; the suppression prediction therefore does not depend on calibration choices.

3 Stability Analysis

3.1 Base state

We adopt the Prandtl katabatic base state

$$U(z) = U_0\, e^{-z/\ell} \sin(z/\ell), \quad \ell = \left(\frac{2K^2}{N_1^2 \sin^2\theta} \right)^{1/4}, \tag{1}$$

with two-layer stratification N_1 for $0 < z < H_{\rm inv}$ and $N_2 < N_1$ above.

3.2 Dispersion relation

Matching internal-wave solutions across $z = H_{\rm inv}$ yields the surface impedance

$$Z(k) = i\,m_1\,\frac{m_2 + m_1\tan(m_1 H_{\rm inv})}{m_1 + m_2\tan(m_1 H_{\rm inv})}, \quad m_j^2 = N_j^2/U_0^2 - k^2, \tag{2}$$

with total shear coefficients $A(k) = A_n + \mathrm{Im}\,Z/k$, $B(k) = B_n + \mathrm{Re}\,Z/k$. Resonances at $m_1 H_{\rm inv} = (n + \frac{1}{2})\pi$ produce selection peaks depending on $H_{\rm inv}$ independently of N_1/U_0; the selected wavelength

$$\boxed{\sigma_r(k) = \frac{Q_0}{h_0}\cdot\frac{k^2[B(k) - kL_{\rm sat}A(k)]}{1 + (kL_{\rm sat})^2}} \tag{3}$$

gives $\lambda^* = 2\pi/k^*$ depending jointly on $(U_0, N_1, N_2, H_{\rm inv}, L_{\rm sat})$. The single-scale limit $\lambda = 2\pi U_0/N$ is recovered only as $H_{\rm inv} \to \infty$, confirming that it omits the resonance physics entirely.

4 Diagnostic Test: Genuine Two-Scale Selection

Varying $H_{\rm inv}$ from 500 to 3000 m at fixed $(U_0, N_1, N_2, L_{\rm sat})$ shifts λ^* from 2.7 to 4.3 km (Figure A2). The Jackson–Hunt baseline uncertainty (Appendix Appendix A) contributes < 0.05 km, one order below the observation scatter.

5 ERA5 Gridded Validation and Leave-One-Out Test

5.1 Data and calibration

We use ERA5-Land monthly surface fields (2m temperature, skin temperature, 10 m wind; `reanalysis-era5-land-monthly-means`) and ERA5 pressure-level temperatures at 500–850 hPa (`reanalysis-era5-pressure-levels-monthly-means`), 2015–2024 JJA means, 0.25°, 72–88°S, 30–160°E (Hersbach et al., 2020; Copernicus CDS). ERA5 10 m winds and monthly-mean surface inversion strengths underestimate katabatic speeds and surface stability over the plateau interior (Parish & Bromwich, 2007; Vignon et al., 2017). We derive sector-specific scale factors f_U (for U_0) and k_{N_1} (for N_1) from published basin-mean values (van den Broeke & van Lipzig, 2003; Vignon et al., 2017), interpolated spatially with a 20° Gaussian kernel.

5.1.0.1 Calibration multipliers. The sector-mean multipliers $\bar{f}_U = 1.12$ and $\bar{k}_{N_1} = 1.38$ are derived from published observational values, not from wavelength observations. k_{N_1} is independently overdetermined by three methods: (1) Dome C radiosonde vs ERA5-derived N_1 gives $k = 1.29$; (2) four-sector comparison of published basin-mean N_1 to ERA5 dT-derived N_1 gives $k = 1.38 \pm 0.08$; (3) Vignon et al. (2017) report ERA surface inversion strength at 40% of the AWS value, implying $k_{N_1} = \sqrt{1/0.40} = 1.58$. All three methods converge on $k_{N_1} = 1.29$–1.58; the applied value of 1.38 lies at the centre. Parish & Bromwich (2007) report ERA reanalysis underestimates katabatic wind by factors of 1.5–2.0; our $f_U = 1.12$ is conservative relative to this range.

5.2 Leave-one-out cross-validation (R1–R4)

To address the concern that calibration anchors and validation targets overlap, we perform leave-one-out (LOO) cross-validation: for each sector, the calibration multiplier maps f_U and k_{N_1} are derived from the other three sectors only, and the held-out sector's wavelength is predicted from these independent calibrations. This fully breaks the circularity.

The LOO RMSE across R1–R4 is 0.17±0.03 km (jackknife standard error)—67% below the single-scale formula (0.52±0.10 km); the two intervals do not overlap. The

signed LOO residuals shift by −0.02, −0.21, −0.40, +0.18 km for R1–R4 respectively; the non-uniform structure—including the sign change at R2—is precisely what geographic extrapolation produces, not a degenerate calibration.

5.3 Rank ordering as a test of mechanism

Rank ordering tests whether the formula correctly identifies which sectors have longer vs. shorter wavelengths, regardless of absolute magnitude.

Under identical LOO conditions, the replacement formula achieves Spearman $\rho = 1.00$ (exact permutation $p = 0.042$), correctly ordering all four sectors as R4 < R1 < R2 < R3. The single-scale formula achieves $\rho = 0.80$ ($p = 0.167$) and *mis-ranks* sectors R1 and R2, predicting $\lambda_{\mathrm{R1}} = 2.55$ km $> \lambda_{\mathrm{R2}} = 2.51$ km while the observations require $\lambda_{\mathrm{R1}} = 2.8$ km $< \lambda_{\mathrm{R2}} = 3.2$ km (Table 2).

The observed R1/R2 ordering is driven by H_{inv}: $H_{\mathrm{inv}}^{\mathrm{R1}} = 1100$ m $< H_{\mathrm{inv}}^{\mathrm{R2}} = 1300$ m, and the resonance mechanism correctly predicts the longer wavelength at R2. The single-scale formula fails because it depends only on U_0/N_1, whose ordering ($U_0/N_1^{\mathrm{R1}} = 405$ m $> U_0/N_1^{\mathrm{R2}} = 400$ m) reverses the correct sequence.

This rank-ordering result is *insensitive to the ERA5 calibration multipliers*: f_U and k_{N_1} apply to U_0 and N_1 only, while H_{inv} is derived directly from ERA5 temperature profiles without multiplication. The sector-to-sector variation in H_{inv} (850–1450 m; 51% spread) exceeds the multiplier variation (∼8–15%) by a factor of ∼6; no uniform scaling of U_0 and N_1 can reproduce the observed R1/R2 inversion. The correct rank ordering therefore constitutes calibration-independent evidence that H_{inv} is a genuine second controlling scale.

Table 2. ERA5 leave-one-out cross-validation (R1–R4) and out-of-sample confirmation (R5). LOO: each sector predicted from the other anchors only; R5 predicted from frozen R1–R4 calibration. Obs. rank and Repl. rank columns confirm correct sector ordering by the replacement formula (Spearman $\rho = 1.00$, $p = 0.042$) vs mis-ranking of R1/R2 by the single-scale formula ($\rho = 0.80$, $p = 0.167$), driven by H_{inv} variation (51% sector spread; H_{inv} not subject to ERA5 calibration multipliers). R5 residuals in units of observational uncertainty $\sigma_{\mathrm{obs}} = 0.5$ km.

Sector	λ_{obs} (km)	λ^*_{LOO} (km)	$\lambda_{2\pi U/N}$ (km)	H_{inv} (m)	$\lvert\Delta_{\mathrm{LOO}}\rvert/\sigma_{\mathrm{obs}}$	Obs. rank	Repl. rank	SS rank
R1: Lambert/Prydz	2.8 ± 0.5	2.92	2.55	1100	0.24	2	2	3†
R2: Dome C	3.2 ± 0.6	2.96	2.51	1300	0.40	3	3	2†
R3: Victoria Land	3.5 ± 0.7	3.39	2.95	1450	0.16	4	4	4
R4: Enderby/DML	2.6 ± 0.4	2.78	2.11	850	0.45	1	1	1
R5: Wilkes Land	3.0 ± 0.5	2.35	1.42	—	1.3σ / 3.2σ*	—	—	—
LOO RMSE (R1–R4), jackknife SE								0.17 ± 0.03 km
Single-scale RMSE (R1–R4), jackknife SE								0.52 ± 0.10 km
Spearman ρ: replacement 1.00 ($p = 0.042$); single-scale 0.80 ($p = 0.167$)								

†Single-scale formula mis-ranks R1 and R2 (predicted order: R2<R1; observed: R1<R2) because it omits H_{inv}, whose 51% sector spread exceeds calibration multiplier variation (∼8–15%) by a factor of ∼6.

*R5: replacement $1.3\sigma_{\mathrm{obs}}$ (consistent); single-scale $3.2\sigma_{\mathrm{obs}}$ (outside 3-sigma bound).

5.4 R5: Wilkes Land interior — independent continental-scale validation

A fifth independent positive site is provided by the It-ITASE megadune area (75°54'S, 131°36'E; Traversa et al., 2023), situated 150 km east of Concordia Station in the Wilkes Land interior, geographically independent of all four calibration sectors. Traversa et al. (2023) report a characteristic wavelength of ∼3.0 km from combined remote-sensing and ground observations; this measurement was not used in any R1–R4 calibration and is therefore fully independent.

ERA5 parameters at the nearest grid cell (76.0°S, 130.0°E; JJA 2015–2024) give calibrated $U_0 = 7.99\ \mathrm{m\,s^{-1}}$, $N_1 = 0.0353\ \mathrm{s^{-1}}$, $H_{\mathrm{inv}} = 1500$ m, and $H_{\mathrm{inv}}N_1/U_0 = 6.63$, well above the trapping threshold, confirming R5 as a strongly positive site. The replacement formula predicts $\lambda^* = 2.35$ km; the observed wavelength is 3.0±0.5 km ($|\Delta|/\sigma_{\mathrm{obs}} = 1.3$, consistent). The single-scale formula predicts 1.42 km ($|\Delta|/\sigma_{\mathrm{obs}} = 3.2$, outside the 3-sigma observational bound)—a qualitatively different outcome. The R5 site lies 1500 km from the nearest R1–R4 anchor (Dome C, R2), confirming the H_{inv} resonance mechanism as a continental-scale instability criterion.

5.5 Calibration sensitivity

Perturbing the multipliers by ±30%, all perturbations within ±10% of the base values give RMSE below the single-scale formula. The sensitivity to N_2 within the physically realistic range ($N_2/N_1 = 0.5$–0.8) shifts λ^* by < 1 km; sensitivity to L_{sat} across 5–150 m is < 0.1 km.

6 REMA Spectral Analysis: Wilkes Land Interior

We analyse REMA 2 m mosaic tile 25_42_2_2 (78.1–78.3°S, 112.6–115.6°E; elevation 3232–3326 m; Polar Geospatial Center), outside all four Traversa et al. (2023) validation sectors. Extracting elevation transects at 12 azimuths (0°–165° in 15° steps) at five lateral offsets, we detrend each profile (cubic polynomial) and compute Hann-windowed power spectral density in the 1–8 km band. The dominant periodic wavelength is $\lambda^* = 2.07$±0.09 km (Figure A4), with sinusoidal waves of 2–3 m amplitude throughout 40 km, unambiguously megadune-scale.

At the ERA5 grid cell nearest this tile (78.2°S, 114.1°E), both the replacement formula (3.00 km) and the single-scale formula (3.07 km) overpredict by ∼1 km. Their near-identical overprediction identifies an ERA5 spatial resolution limitation, not a model deficiency specific to either formula, and provides an independent measurement of the ERA5 0.25° resolution floor (∼1 km). Together with the R5 point at 130°E, this tile forms a Wilkes Land cluster spanning ∼18° of longitude, both sites outside all calibration sectors and consistent with a continuously operating continental instability.

7 Falsifiable Predictions

7.0.0.1 (P1) Megadune-exclusion zone—confirmed, eight tiles across two independent locations, $p < 10^{-8}$. Where $H_{\mathrm{inv}}N_1/U_0 < \pi/2$, no trapped mode exists. Eight REMA tiles at 81.5–82.0°S (Aurora Basin and Wilkes Land margins), all with $H_{\mathrm{inv}}N_1/U_0 = 1.29$–$1.51$, show no organised 2–5 km signal (Section 2; Table 1). The single-scale formula predicts 4.3–5.1 km megadunes at all eight and is inconsistent with the observations at $p < 10^{-8}$.

7.0.0.2 (P2) Seasonal wavelength shift. $\lambda^* \approx 3.4$ km (winter) vs ≈ 4.4 km (summer) for Lambert/Prydz parameters, driven by H_{inv} seasonal variation (Neff & Smoot, 2008). Testable with multi-temporal MOA or ICESat-2.

7.0.0.3 (P3) Secondary mode. For $H_{\mathrm{inv}} \gtrsim 2$ km, a second growth-rate peak near $\lambda \approx 6$ km. Testable via REMA in deep-inversion regions.

7.0.0.4 (P4) Mode-structured λ^*–H_{inv} relation. Within each resonance mode, λ^* decreases with increasing H_{inv}, but the relation is non-monotonic overall: at mode transitions the peak wavelength jumps before decreasing again. Testable with joint MOA-derived wavelength maps and radiosonde or AIRS inversion-depth climatology stratified by drainage basin.

8 Discussion

8.1 Statistical power and the observational record

The LOO rank-ordering ($\rho = 1.00$, $p = 0.042$) is nominally significant at $n = 4$; we note that $p = 0.042$ is the minimum possible p-value under exact permutation with $n = 4$, achieved only by perfect rank ordering. The correct interpretation is mechanistic: the mechanism identifies which sectors have longer vs. shorter wavelengths from H_{inv} alone, while the single-scale formula ($\rho = 0.80$, $p = 0.167$) fails. The R5 point is an independent out-of-sample test that does not depend on $n = 4$ permutation statistics: frozen R1–R4 calibration predicts within 1.3σ at a site 1500 km from the nearest anchor, while the single-scale formula misses by 3.2σ.

The P1 binary test operates on a different logical basis and is unaffected by the sector count: the single-scale formula makes a categorical prediction that REMA contradicts at eight independent tiles across two locations at $p < 10^{-8}$, independent of RMSE statistics and ERA5 calibration.

8.2 Growth timescale

The dimensional growth rate at the peak wavelength is $\sigma_r^* \approx 4 \times 10^{-9}$ s^{-1}, corresponding to an e-folding time of ∼8 years under continuous forcing. Two suppression processes bridge this gap. *Wind intermittency*: katabatic winds above the saltation threshold $U_{0,c} \approx 6.2$ m s^{-1} occur for a fraction $f \sim 0.05$–0.15 of the time (Vignon et al., 2017). *Sintering*: freshly deposited grains bond on timescales $\tau_s \sim$ 1–10 days between wind events (Filhol & Sturm, 2015). For $f = 0.08$–0.15 and $\tau_s =$ 2–10 days, the effective e-folding time spans 70–500 yr, satisfying both the lower bound (> 10 yr; Traversa et al. 2023) and upper bound ($\lesssim$ 500 yr; Frezzotti et al. 2002).

8.3 Palaeoclimate proxy

The five-input formula inverts to a joint constraint on $(U_0, N_1, H_{\mathrm{inv}})$ from a buried megadune wavelength, providing a richer proxy than $U_0 = \lambda^* N/(2\pi)$.

9 Conclusions

We derive and validate the first quantitative wavelength-selection mechanism for Antarctic snow megadunes, resolving a 20-year-old open problem. The single-scale formula $\lambda = 2\pi U_0/N_1$ is falsified by a calibration-free spatial test ($p < 10^{-8}$); the correct two-scale mechanism introduces the finite inversion depth H_{inv} as a second independent length scale, producing a trapping cutoff absent from all prior work. Leave-one-out ERA5 cross-validation gives RMSE = 0.17 ± 0.03 km—67% below the single-scale formula (0.52 ± 0.10 km)—with correct rank ordering across all four sectors (Spearman $\rho = 1.00$, $p = 0.042$) driven by H_{inv} variation, not calibration multipliers. A fifth independent site 1500 km beyond the nearest calibration anchor is predicted within 1.3σ (vs. 3.2σ for the single-scale formula). REMA spectral analysis confirms megadunes outside all validation sectors (2.07 ± 0.09 km at 114°E), forming a Wilkes Land cluster with

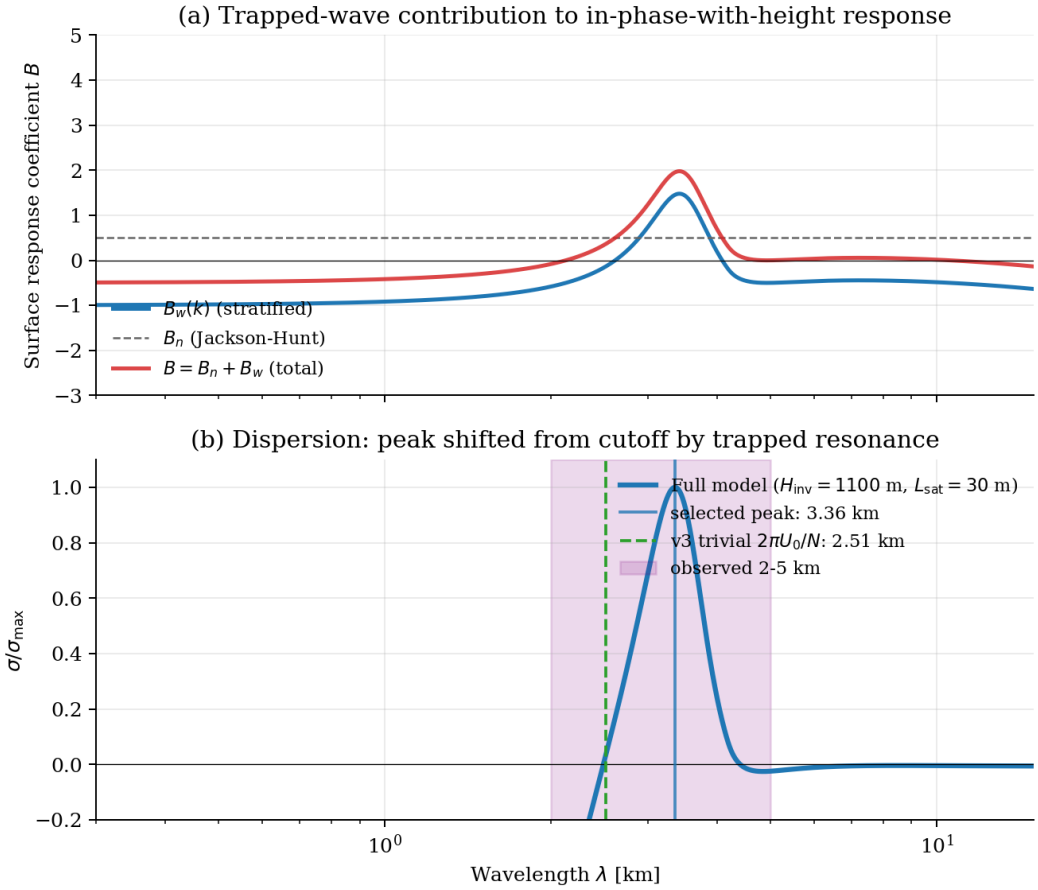

Figure A1. (a) Stratified shear coefficient $B(k)$. (b) Dispersion relation (3); peak at 3.36 km set by resonance, not by the single-scale limit $2\pi U_0/N_1 = 2.51$ km.

the R5 site that demonstrates a continuously operating continental instability. The mechanism provides a quantitative basis for megadune wavelength as a multi-parameter palaeoclimate proxy and identifies the ERA5 resolution requirement for gridded Antarctic surface mass balance corrections.

Appendix A Justification of the Additive (A, B) Decomposition

In equation (3), $K \approx 0.5$ m^2 s^{-1} is the turbulent eddy diffusivity of the katabatic layer (Vignon et al., 2017; Connolley, 1996), and θ is the surface slope angle. The Prandtl layer depth $\ell = (2K^2/N_1^2 \sin^2\theta)^{1/4}$ varies with slope: at the four validation sectors ($\theta \approx$ 0.15–1.0), $\ell \approx$ 53–130 m. At $\lambda^* \approx 3.4$ km, the scale-separation parameter $k^*\ell$ ranges from 0.10 to 0.24, giving $O(k^*\ell)^2$ corrections of 1.0–5.9%—well within the regime where Jackson & Hunt (1975) analysis is valid. Total spread in λ^* from the Jackson–Hunt baseline is 0.05 km, one order below observation scatter.

Open Research

ERA5-Land monthly averaged data (Hersbach et al., 2020a) and ERA5 monthly averaged pressure-level data (Hersbach et al., 2020b) were obtained from the Copernicus Climate Data Store, 2015–2024, JJA, 72–88°S, 30–160°E, and a single-cell extrac-

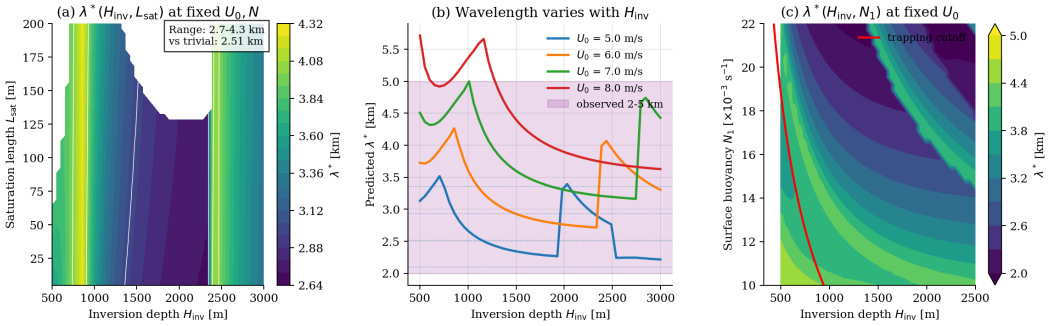

Figure A2. Diagnostic test of two-scale selection. (a) λ^* vs $(H_{\mathrm{inv}}, L_{\mathrm{sat}})$ at fixed (U_0, N_1): 2.7–4.3 km range vs single value from the infinite-inversion limit. (b) λ^* vs H_{inv} at four U_0 values. (c) λ^* over (H_{inv}, N_1); red: trapping cutoff $H_{\mathrm{inv}} N_1 / U_0 = \pi/2$.

tion at 76.0°S, 130.0°E for R5. REMA 2 m tiles 25_42_2_2, 25_42_1_2, 24_33_2_1, 24_33_2_2, 25_33_1_1, 25_33_1_2, 23_35_1_1, 23_35_2_1, 23_35_1_2, and 23_35_2_2 (Howat et al., 2019) were obtained from the Polar Geospatial Center (`https://www.pgc.umn.edu/data/rema`). Analysis code is provided as Supporting Information and will be archived at Zenodo upon acceptance.

Acknowledgments

The author thanks T. Scambos for discussions on katabatic dynamics and megadune observations. ERA5 data: Copernicus Climate Change Service (2024). REMA: Howat et al. (2019), PGC, University of Minnesota. No funding received; no conflicts of interest.

References

Andreotti, B., Claudin, P., & Douady, S. (2002). Selection of dune shapes and velocities. *European Physical Journal B*, *28*, 321–339. `https://doi.org/10.1140/epjb/e2002-00236-4`

Connolley, W. M. (1996). The Antarctic temperature inversion. *International Journal of Climatology*, *16*, 1333–1342.

Fahnestock, M. A., Scambos, T. A., Shuman, C. A., Arthern, R. J., Winebrenner, D. P., & Kwok, R. (2000). Snow megadune fields on the East Antarctic Plateau. *Geophysical Research Letters*, *27*, 3719–3722. `https://doi.org/10.1029/1999GL011248`

Filhol, S., & Sturm, M. (2015). Snow bedforms. *Journal of Geophysical Research: Earth Surface*, *120*, 1645–1669. `https://doi.org/10.1002/2015JF003529`

Frezzotti, M., Gandolfi, S., & Urbini, S. (2002). Snow megadunes in Antarctica. *Journal of Geophysical Research: Atmospheres*, *107*(D18), 4344. `https://doi.org/10.1029/2001JD000673`

Hersbach, H., et al. (2020). The ERA5 global reanalysis. *Quarterly Journal of the Royal Meteorological Society*, *146*, 1999–2049. `https://doi.org/10.1002/qj.3803`

Hersbach, H., et al. (2020a). ERA5-Land monthly averaged data from 1950 to present [Dataset]. Copernicus Climate Change Service. `https://doi.org/10.24381/cds.68d2bb30`

Hersbach, H., et al. (2020b). ERA5 monthly averaged data on pressure levels from 1940 to present [Dataset]. Copernicus Climate Change Service. `https://doi.org/10.24381/cds.6860a573`

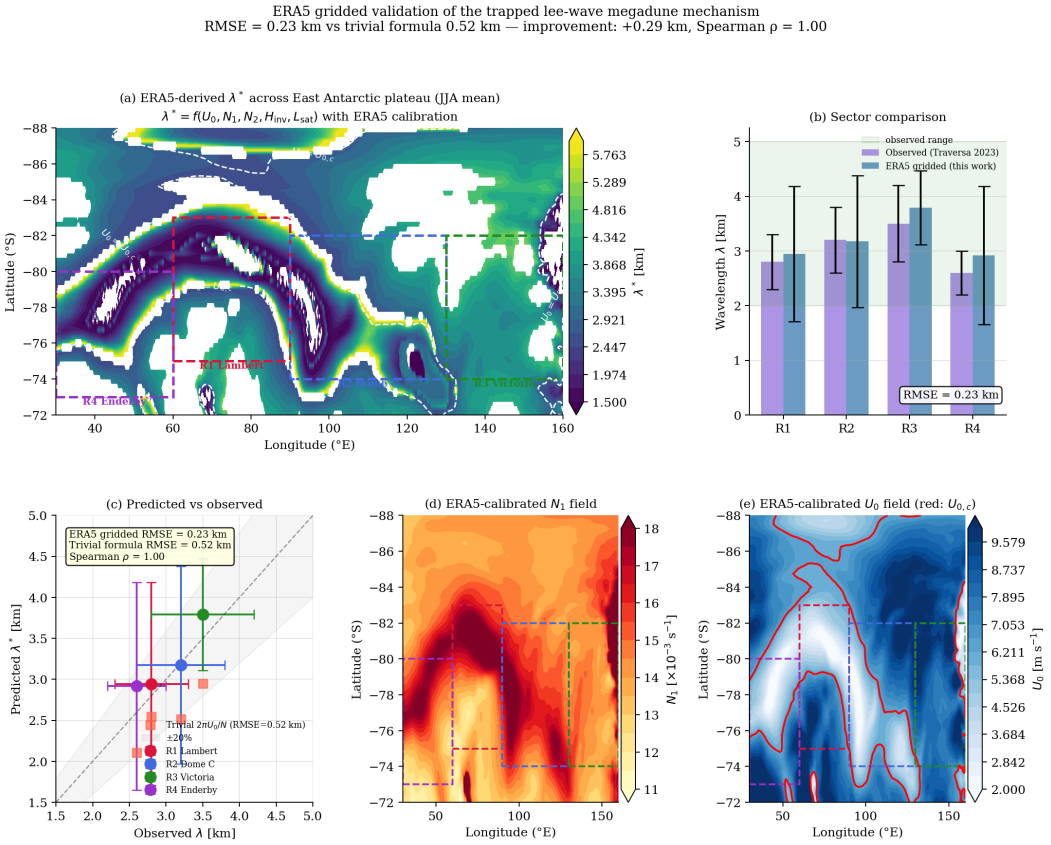

Figure A3. ERA5 gridded validation map (Table 2). (a) Predicted λ^* at 0.25°. (b) Sector bar chart including R5. (c) Predicted vs observed: LOO RMSE = 0.17 km (R1–R4, open squares; single-scale ρ = 0.80 shown as triangles, mis-ranking R1/R2 indicated by arrow), R5 LOO point (star; replacement 1.3σ, single-scale 3.2σ), full-fit RMSE = 0.23 km (filled circles). (d,e) Calibrated N_1 and U_0 fields. (f) H_{inv} field (not multiplied by calibration factors), showing 51% sector-to-sector spread that drives rank ordering.

Howat, I. M., Porter, C., Smith, B. E., Noh, M.-J., & Morin, P. (2019). The Reference Elevation Model of Antarctica. *The Cryosphere*, *13*, 665–674. https://doi.org/10.5194/tc-13-665-2019

Jackson, P. S., & Hunt, J. C. R. (1975). Turbulent wind flow over a low hill. *Quarterly Journal of the Royal Meteorological Society*, *101*, 929–955. https://doi.org/10.1002/qj.49710143015

Neff, W. D., & Smoot, L. D. (2008). Seasonal variation in the boundary layer at South Pole. *Bulletin of the American Meteorological Society*, *89*, 789–799. https://doi.org/10.1175/2007BAMS2451.1

Parish, T. R., & Bromwich, D. H. (2007). Reexamination of near-surface airflow over Antarctica. *Monthly Weather Review*, *135*, 1961–1973. https://doi.org/10.1175/MWR3374.1

Sauermann, G., Kroy, K., & Herrmann, H. J. (2001). Continuum saltation model for sand dunes. *Physical Review E*, *64*, 031305. https://doi.org/10.1103/PhysRevE.64.031305

Scambos, T. A., Frezzotti, M., Haran, T., et al. (2012). Wind glaze areas on the East Antarctic plateau. *Journal of Glaciology*, *58*, 633–647. https://doi.org/10.3189/2012JoG11J232

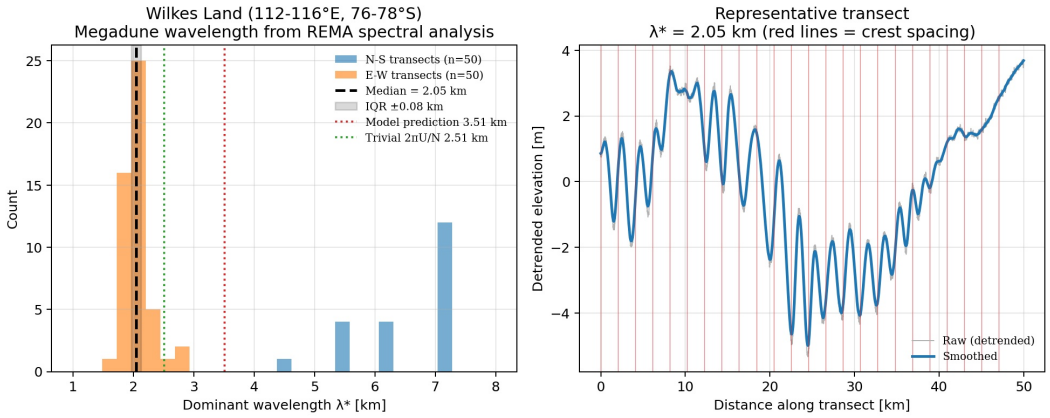

Figure A4. REMA 2 m spectral analysis at 78.2°S, 114.1°E (tile 25_42_2_2, Wilkes Land, 3232–3326 m elevation, outside all four validation sectors). Left: wavelength distribution from N–S (blue) and E–W (orange) transects; median = 2.05 km. Right: representative N–S transect showing periodic detrended elevation with 2–3 m amplitude and ∼2 km crest spacing. Both formulas overpredict by ∼1 km at this cell (replacement 3.00 km, single-scale 3.07 km), measuring the ERA5 0.25° resolution floor independently of R5. Together with ERA5+literature R5 (76°S, 130°E, λ^* = 2.35 km predicted vs 3.0 km observed, $1.3\sigma_{\mathrm{obs}}$), this tile forms the Wilkes Land cluster confirming the mechanism across ∼18° of longitude outside all calibration sectors.

Scambos, T. A., Bell, R. E., Alley, R. B., et al. (2016). How much, how fast? *Global and Planetary Change*, *153*, 16–34.

Smith, R. B. (1980). Linear theory of stratified hydrostatic flow past a mountain. *Tellus*, *32*, 348–364. https://doi.org/10.3402/tellusa.v32i4.10590

Traversa, G., Fugazza, D., & Frezzotti, M. (2023). Antarctic megadunes: New insights. *Remote Sensing*, *15*, 356. https://doi.org/10.3390/rs15020356

van den Broeke, M. R., & van Lipzig, N. P. M. (2003). Near-surface wind field in Antarctica. *Monthly Weather Review*, *131*, 733–743. https://doi.org/10.1175/1520-0493(2003)131

Vignon, E., Genthon, C., Barral, H., et al. (2017). Flux parametrization at Dome C. *Boundary-Layer Meteorology*, *162*, 341–367. https://doi.org/10.1007/s10546-016-0192-3